Micromachined Fabry-Perot cavity pressure transducer with optical fiber interconnects

Youngmin Kim and Dean P. Neikirk

The University of Texas at Austin, Department of Electrical and Computer Engineering
Microelectronics Research Center
Austin, TX 78712

ABSTRACT

A monolithically integrated Fabry-Perot cavity pressure transducer has been fabricated using micromachining techniques that are fully compatible with silicon IC processing technology. Surface micromachining can produce a high quality micro cavity without the wafer bonding process that has been commonly used in previously fabricated Fabry-Perot pressure transducers. Dielectric film stacks consisting of layers of silicon nitride and silicon dioxide were used as mirrors. An air gap cavity was formed by selectively etching a sacrificial polysilicon layer. Remote pressure measurement was demonstrated using the micromachined Fabry-Perot cavity and a multimode optical fiber interconnect. The measured response of the sensor has been compared with theoretical simulation which takes into account the averaging effect caused by the shape of the deflected mirror in the cavity.

Keywords: micromachined Fabry-Perot cavity, pressure sensor, multimode optical fiber interconnect

2. INTRODUCTION

Fabry-Perot cavity-based sensors have been widely studied for their versatility; for example they have been used to sense both pressure and temperature [1, 2]. This kind of sensor, usually combined with optical fibers, detects changes in optical path length induced by either a change in the refractive index or a change in physical length of the cavity. Unlike "intrinsic" optical fiber sensors where the fiber is itself the sensing element, in this "extrinsic" system a cavity is used as a sensing element and optical fiber is used as an interconnect [3]. Advantages of this extrinsic system include high sensitivity and localized measurement. The Fabry-Perot cavity based sensors also have some advantages over piezoresistive and capacitive sensors. For example, remote data acquisition can be achieved using the cavity based sensors without degradation of signal to noise ratio due to electromagnetic interference. For piezoresistive and capacitive sensors, on-sensor-chip electronics integration is usually necessary to improve signal to noise ratio (S/N ratio). Even for piezoresistive sensors, additional electronics are commonly required for correcting the offset and sensitivity to temperature coefficients. Using a micromachined Fabry-Perot cavity transducer and an optical fiber interconnect these problems can be avoided. In addition, compared with capacitive pressure sensors, the dimensions of an optical sensing element, such as the Fabry-Perot cavity discussed here, can be made much smaller. Practically, however, it has been very hard to construct high quality Fabry-Perot cavity sensors due to the immaturity of their fabrication techniques. Thus Fabry-Perot cavity based sensors were not commercially realized until the mid 80's, even though the basic principle has been long recognized.

Meanwhile, micromachining techniques have rapidly been developed over the last two decades for their great impact on microsensors [4, 5] and microelectromechanical systems [6]. Compatibility with VLSI technology allows microstructures to be integrated with driving circuits or signal conditioning circuits on the same chip, improving functionality of the microstructures [7] and reducing noise problems. Micromachining techniques also make Fabry-Perot cavity based devices more attractive by reducing the size and the cost of the sensing element.

One commonly used method of building a micro Fabry-Perot cavity is a hybrid assembly technique using a fusion bonding process. Using this technique Fabry-Perot cavity based devices, such as tunable filters [8] and pressure sensors [9, 10], have been demonstrated. However, a high quality micro Fabry-Perot cavity frequently requires an elaborate fusion bonding process, that may lead to low manufacturing yield. As an alternative, surface micromachined Fabry-Perot cavity based devices have recently developed. Among these devices are a tunable interferometer [11] and a pressure sensor [12]. Surface

0-8194-2008-5/95/$6.00

micromachining techniques eliminate the fusion bonding step and instead etch a sacrificial layer to form a high quality cavity with an air gap, achieving higher yield and better performance through precisely controlled thickness of the cavity gap.

In this paper a new fabrication technique for a micro Fabry-Perot cavity based pressure sensor is discussed. The fabrication technique utilizes surface and bulk micromachining to form a cavity with two flexible mirrors. The micromachined cavity, combined with a multimode optical fiber interconnect, has been used to measure differential pressure. To simulate the optical response of the cavity, the deflection of the mirror in the cavity has also been calculated using a numerical method, and excellent agreement between simulations and measurements has been achieved.

3. DESIGN

To build a micromachined Fabry-Perot cavity pressure sensor, a fabrication process is required that can produce four major components (Fig. 1) : a "top" diaphragm that also serves as one of the mirrors of the Fabry-Perot cavity; an air gap between the mirrors of the cavity; a "bottom" diaphragm that forms the other mirror; and a mechanical structure that holds and aligns the optical fiber to the micromachined cavity. The design of the sensor consists primarily of selecting the appropriate layer thicknesses and lateral dimensions for each of these components. Both mechanical and optical characteristics should be considered in the design process.

We first consider the mechanical reliability of the diaphragms/mirrors. Due to residual stress of deposited films, a diaphragm made of the deposited films can suffer from cracking or buckling. To avoid deformation of the diaphragm, a multiple film stack, consisting of films under compressive residual stress and under tensile residual stress, has been used. The composite stack has less equivalent stress by compensating the compressive (or tensile) stress of films with the tensile (or compressive) stress of other films. Equivalent residual stress of a composite film stack can be obtained using the equation [13]

$$\sigma_{eq} = \frac{\sum_i (\sigma_i \cdot h_i)}{\sum_i h_i}, \qquad (1)$$

where σ_i is the residual stress and h_i the thickness of the i^{th} film. The thickness of each layer is chosen so that the equivalent residual stress of the composite stack is slightly under tension. Here a multiple stack consisting of silicon nitride and silicon dioxide was used as a diaphragm/mirror. Residual stresses of silicon nitride and silicon dioxide deposited by LPCVD (Low Pressure Chemical Vapor Deposition) were estimated using the beam curvature method. The silicon nitride and silicon dioxide had 1.3 GPa tensile stress and 0.3 GPa compressive stress, respectively. Based on the residual stress of the films, the thickness of each layer in the mirror can be selected.

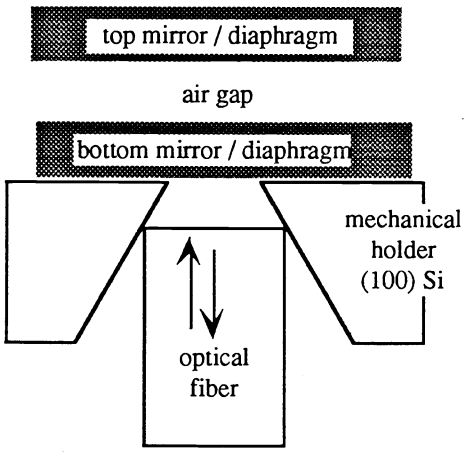

Figure 1: Schematic diagram of the components necessary for the micromachined Fabry-Perot pressure sensor.

In addition to mechanical stability of the diaphragm/mirrors, the optical characteristic of the mirror is a function of the thickness of each layer. For pressure sensor applications it is often desirable to maximize the distance a mirror can move while producing an approximately linear change in reflectance. This suggests the use of a moderately low finesse cavity, using dielectric mirrors that do not individually produce high reflectances (e.g., they should not consist of quarter wavelength stacks). Thus, the cavity reflectance is not extremely sensitive to mirror layer thicknesses, allowing us to choose these thicknesses to satisfy the mechanical constraint of low equivalent stress discussed above.

Besides mirror reflectivity, the initial gap (i.e., the gap at zero applied pressure) between the two mirrors of the Fabry Perot cavity, as well as the mechanical travel of the moving mirror, are also part of the design of the pressure sensor. Determination of these dimensions usually require additional constraints imposed by either desired pressure range or the manufacturing process. For example, these design variables (i.e., travel and initial gap) should be carefully selected to maximize yield when layer

thickness variation due to the manufacturing process is considered [14] With a proper combination of initial cavity length and mechanical travel the optical response of the cavity becomes the least sensitive to process-induced thickness variations in the layers of the cavity .

The fourth structure needed for the design serves to hold and align the optical fiber interconnect to the micromachined Fabry-Perot cavity. If the lateral size of the bottom diaphragm is larger than the optical fiber it becomes very difficult to place the fiber against the diaphragm without breakage. However, if the anisotropically etched hole through the (100) silicon wafer is sized so that the bottom diaphragm is smaller than the fiber, the walls of the pyramidal hole can serve as a mechanical stop, as illustrated in Fig. 1. Experimentally, we have found that with such a configuration the fiber self-aligns to the diaphragm as it is forced into the etched hole. Once the fiber has "bottomed out" in the hole, small forces applied transverse to the fiber axis produce no observable change in optical response, indicating the fiber is locked into place by contact with the four walls of the hole. The fiber can be repeatedly removed and re-inserted, each time producing essentially identical optical response.

The constraints discussed above primarily determine the layer thicknesses in the Fabry-Perot structure and the lateral size of the bottom diaphragm. The relationship between desired pressure range and mechanical travel is set by the compliance of the pressure-deflected diaphragm. This in turn is determined by the thickness and lateral dimensions of the diaphragm that forms the moving mirror in the transducer. Depending on the fabrication process used, either the top or the bottom diaphragm can be made the moving mirror. In the fabrication process shown below, the bottom diaphragm forms the moving mirror, and since the lateral dimensions are set by the fiber alignment structure, compliance would be adjusted mainly via changes in the diaphragm thickness.

4. FABRICATION

Lightly doped 4-inch single crystal (100) silicon wafers were used as a substrate. The wafers were either p-type or n-type and 300 μm thick. Before deposition of dielectric layers on the wafers, the wafers were cleaned using the piranha cleaning process. After the piranha cleaning, multiple dielectric films were deposited using LPCVD. The multiple film stack consists of two silicon nitride layers cladding a silicon dioxide layer and will be the bottom diaphragm/mirror of the Fabry-Perot cavity. Silicon nitride was formed by reaction of ammonia (NH_3) and dichlorosilane ($SiCl_2H_2$) at the relative gas flow rate of 3.5:1 at $800\,^{o}C$ and 220 mTorr. Silicon dioxide was formed by reaction of silane (SiH_4) and oxygen (O_2) at the relative gas flow rate of 3:4 at $450\,^{o}C$ and 110 mTorr. To monitor the thickness of deposited films accurately, two bare wafers were placed into the two slots adjacent to the slot the wafer with the devices was in.

Taking both the mechanical reliability and the optical response into account, two 1600 Å thick silicon nitride layers and a 4600 Å thick silicon dioxide layer were deposited as a bottom mirror. After the deposition of the bottom mirror, the dielectric film stack on the back side of the wafer was patterned using Reactive Ion Etching (RIE) to form etch windows for subsequent wet etching. With a photoresist mask, the silicon dioxide and silicon nitride layers were dry-etched using CF_4 and O_2. After patterning the etch windows, the silicon substrate was anisotropically etched using either KOH or EDP to form the bottom diaphragm. Etching was carried out without stirring in a glass vessel at 80 ^{o}C. A reflux condenser unit was used to avoid the changes in the concentration of the etch solution during etching. The maximum size of the bottom diaphragm is limited by the size of the optical fiber which will be used as an interconnect and inserted from the back side of the wafer. To make the fiber contact on the (111) planes as shown in Figure 1, instead of directly contacting the bottom diaphragm, the size of the diaphragm should be smaller than the diameter of the fiber (145 μm).

After making the bottom diaphragm, alignment keys were patterned with respect to the bottom diaphragm on the front side of the wafer before deposition of the polysilicon layer. This step is quite necessary to make it possible to align to the bottom diaphragm after the deposition of the polysilicon layer. Otherwise, the bottom diaphragm can hardly be seen from the front side of the wafer after the deposition of the polysilicon layer. Even with 0.5 μm thick polysilicon layer most of the light is reflected from the top of the polysilicon or absorbed inside the polysilicon layer, making it impossible to align a mask with respect to the bottom diaphragm from the front side of the wafer. To pattern the alignment keys in the dielectric layers, the dielectric layers were dry-etched with a photoresist mask using RIE for 1 minute under the conditions described above.

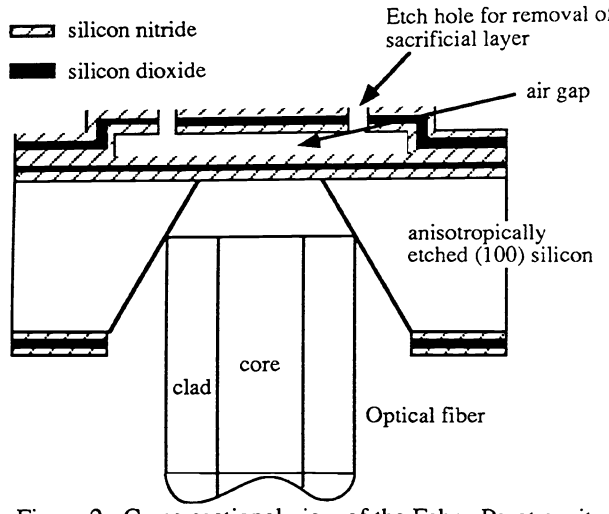

Figure 2: Cross-sectional view of the Fabry-Perot cavity sensor with two flexible dielectric mirrors.

To prevent deposition on the back side of the bottom diaphragm, a dummy wafer was placed in the same slot as the wafer with devices to cover the back side of the wafer. A 6000 Å thick polysilicon layer was deposited by LPCVD at 650 ^{o}C using silane (SiH_4) and patterned using the predefined alignment keys. After patterning the polysilicon layer, another dielectric film stack, which consisted of two 600 Å thick silicon nitride layers cladding a 4200 Å thick silicon dioxide layer, was deposited on the pre-patterned polysilicon. This dielectric stack forms the top mirror and is freed after etching the polysilicon layer. Again, the thickness of each film was chosen to reduce the total residual stress of the stack. After the deposition of the top mirror, a photoresist layer was patterned for the etch windows to allow access to the sacrificial layer. The etch windows were formed in the top mirror using RIE. Upon removal from RIE chamber, the sacrificial layer, i.e. polysilicon, was etched using KOH. To avoid sticking problems, the wafers were finally rinsed with methanol before being dried. Figure 2 shows a cross section of a complete Fabry-Perot cavity coupled to an optical fiber.

5. MEASUREMENTS AND DISCUSSIONS

The optical transmittance of the Fabry-Perot cavity with air gap was measured as a function of wavelength in "free space" using a collimated illumination source (Fig. 3). The transmittance of the cavity was also calculated with the characteristic matrix method [15], assuming plane waves propagate through the dielectric layers at normal incidence, using the layer thicknesses given above. Included in the simulation is the variation of the refractive index of each film as a function of wavelength, using the data from [16]. The agreement between the measurement and the simulation indicates the refractive indices of silicon nitride and silicon dioxide prepared using LPCVD are consistent with the previously published values [16].

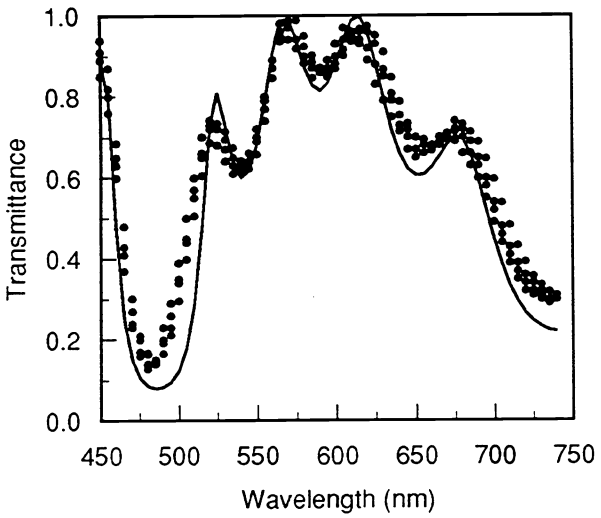

Figure 3: Transmittance of the Fabry-Perot cavity described in the text as a function of wavelength; dots: measured response; solid line: simulated response.

After transmittance measurement, a differential pressure was applied across the cavity while monitoring the transmitted light intensity. Since the top diaphragm has etch holes, the differential pressure deflected the bottom diaphragm causing the cavity length to change. The transmittance of the cavity was measured at various wavelengths as the pressure was varied. For the simulation of the transmittance of the cavity, the shape of the bottom diaphragm must be found because the deflection of the diaphragm is not uniform over the optically sampled area due to the nearly equal size of the fiber core and bottom diaphragm. The deflection of the bottom diaphragm was calculated using a numerical method, i.e. Marcuse method [17]. For the calculation, the equivalent Young's Modulus and residual stress was assumed to be 170 GPa and 0.3 GPa tensile stress, respectively. When a differential pressure (P) is applied to the diaphragm, the equation for the deflection is

$$\omega = \frac{K}{236.7}\{1 - 0.219\cosh(2.556\xi) + 0.0002\cosh(8.51\xi)\}$$
$$\times\{1 - 0.219\cosh(2.556\varphi) + 0.0002\cosh(8.51\varphi)\} \quad (2)$$

where $K = \frac{a^4 \cdot P}{16D}$, $\xi = \frac{2x}{a}$, $\varphi = \frac{2y}{a}$, and D and a are flexural rigidity and length of the diaphragm, respectively. A contour map of the deflection shown in equation (2) is plotted in Figure 4.

The shape of the deflected diaphragm was used to find the fraction of the optically sampled area at each gap. A weighted average transmittance T_{avg} can then be calculated from

$$T_{avg} = \frac{\sum[T(g) \cdot A(g)]}{\sum A(g)} \quad (3)$$

where $T(g)$ is the reflectance of the cavity at gap g and $A(g)$ is the area with cavity gap g. The measurement and simulation of the transmittance of the cavity are plotted as a function of pressure in Fig. 5. In the figure, the transmittance at wavelengths of 630 and 490 nm are chosen for purpose of illustration. Note that the transmittance curves do not have a period of one half the illumination wavelength due to the non-uniform shape of the deflected diaphragm.

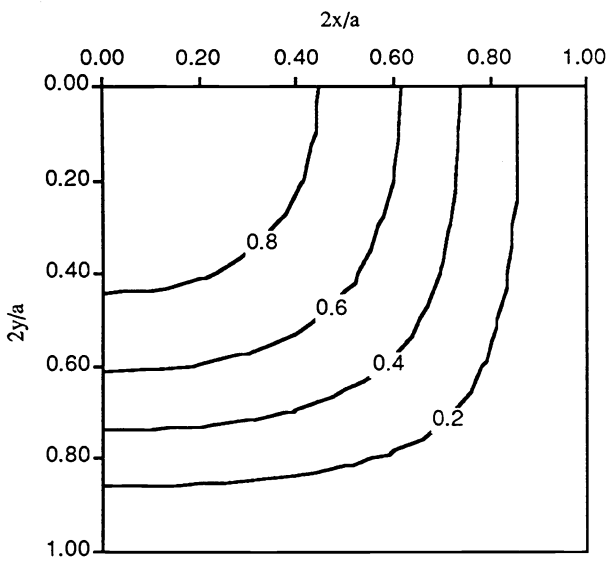

Figure 4 : Normalized deflection contour map of the bottom diaphragm having 0.3 GPa residual stress and 170 GPa Young's Modulus. The origin of the coordinates corresponds to the center of the diaphragm.

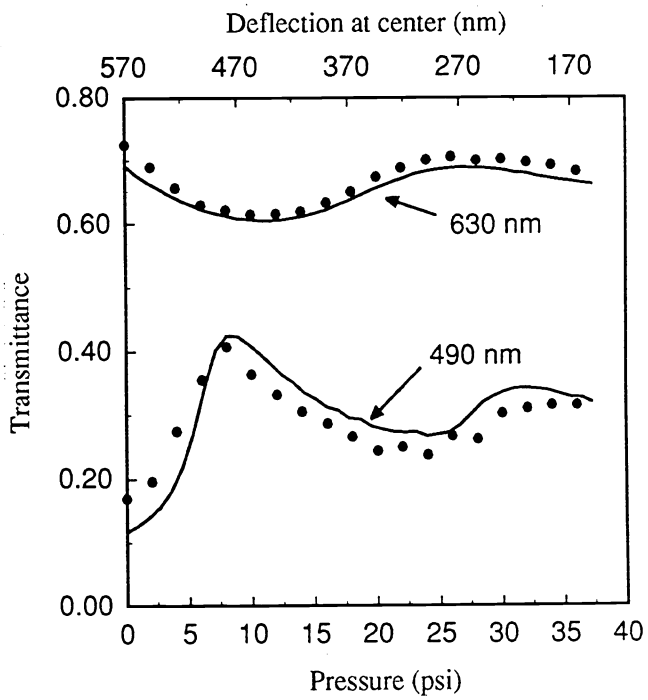

Figure 5: Transmittance of the Fabry-Perot cavity as a function of applied differential pressure. Solid line: simulation; dotted line: measurement.

Remote pressure sensing was achieved by using the micromachined cavity with an optical fiber interconnect. As a measurand, reflectance, instead of transmittance of the cavity, was used to sense changes in the cavity gap. Figure 6 shows a schematic diagram of the experimental setup. A 3 dB optical fiber directional coupler was used as an interconnect and a 633 nm He-Ne laser was used as a light source. The multimode optical fiber had a 100 μm diameter core and a 145 μm diameter cladding layer. For high signal-to-noise (S/N) ratio, a chopper was placed between the laser and the fiber input, and the photocurrent signals produced by the photodetectors were fed into two lock-in amplifiers through transimpedance preamplifiers.

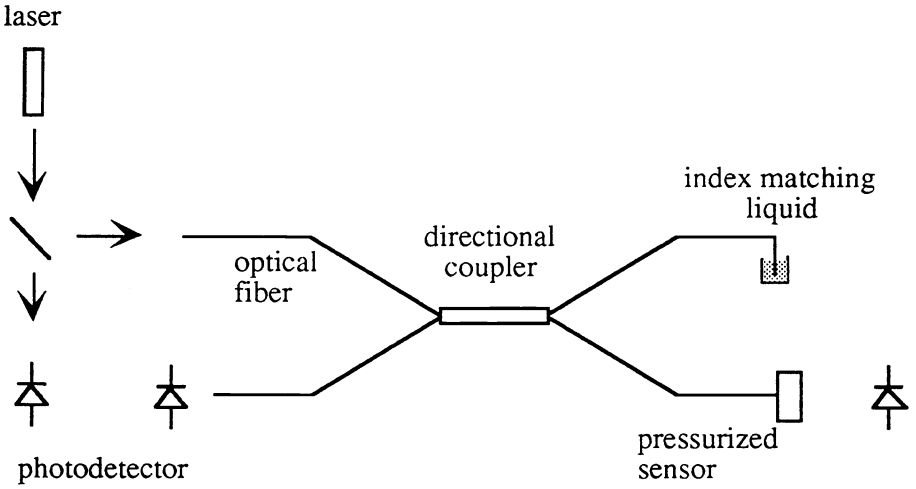

Figure 6: Experimental setup for reflectance measurement of a micromachined Fabry-Perot cavity with an optical fiber interconnect.

The optical fiber was aligned to the Fabry-Perot cavity using the guiding structure formed by anisotropic etching, as shown in Figs. 1 and 2. Since the diameter of the cladding layer is bigger than the width of the bottom diaphragm, there existed a few tens of micron space between the bottom mirror and the fiber when the fiber was bottomed-out in the guiding structure.

Figure 7 shows the measured and simulated reflectance of the Fabry-Perot cavity sensor with a 100 μm x 100 μm bottom diaphragm/mirror as pressure is applied to the device. The simulation took into account the averaging effect of the deflected mirror and used a gap between the bottom mirror and the fiber as a fitting parameter to match the measured curve. Excellent agreement between measured and calculated response was obtained for a fiber / bottom diaphragm gap of 32 μm, consistent with the mechanical dimensions of the fiber and sensor. The normally-incident plane wave model seems to be adequate for this structure even using a multi-mode fiber as the optical interconnect, primarily due the small size of the gaps between the fiber and the cavity, and between the mirrors of the cavity.

6. CONCLUSIONS

A monolithically integrated micro Fabry-Perot cavity has been fabricated using micromachining techniques. The process for the device is compatible with silicon IC technology and avoids the use of wafer bonding. Similar structures could readily be implemented as an optical modulator for fiber communication [18] applications. Remote pressure sensing has also been demonstrated by using the micro pressure-sensitive cavity and a multimode optical fiber as an interconnect. The small cavity gap should allow the microcavity to produce an interferometric effect with even a low coherence length light source, e.g., an LED, and a multimode fiber that could not be used in conventional interferometric devices. One drawback of this particular micromachined cavity is the averaging effect of the optical response caused by variation in the amount of deflection over the optically sampled area. The averaging effect results in smaller dynamic range for the sensing system. The easiest method to reduce the averaging effect is to decrease the optically sampled area, i.e., use a fiber with a smaller core, but this also leads to a weaker reflected signal due to low coupling efficiency. We are currently developing processes with sacrificial etch hole access through the bottom diaphragm, producing a "sealed" top diaphragm. In such a transducer the top diaphragm,

which can be made much larger than the fiber core, becomes the moving mirror. This produces a much more uniform deflection over the optically sample area, increasing the sensitivity of the sensor.

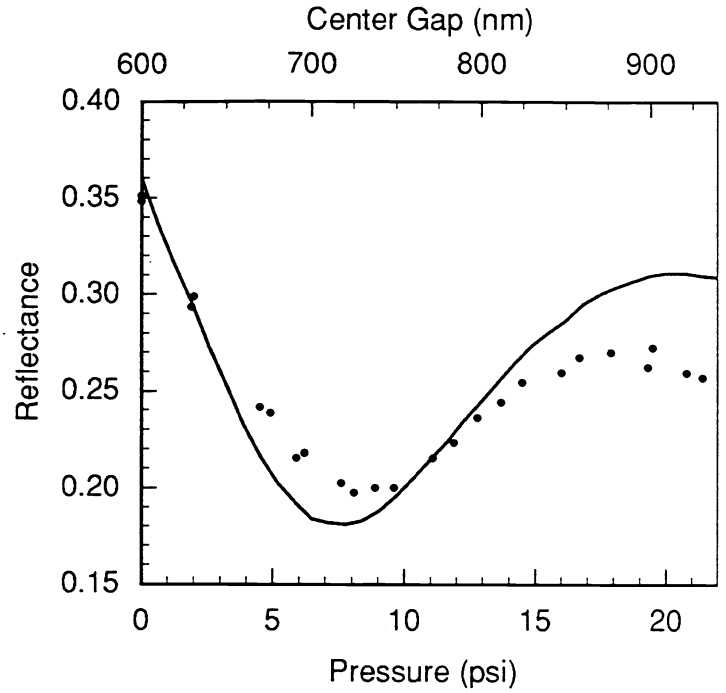

Figure 7: Reflectance of Fabry-Perot cavity as a function of pressure; dots: measured response; solid line: simulated reflectance averaged over the shape of the bent mirror, as a function of the gap at the center of the mirror.

7. ACKNOWLEDGMENTS

This work was sponsored by the Advanced Research Projects Agency (ARPA) Embedded Microsystems Program under contract # DABT63-92-C-0027 AMD P00002- DOD-ARPA.

8. REFERENCES

1. C. E. Lee and H. F. Taylor, "Fiber-optic Fabry-Perot Temperature Sensor Using a Low-Coherence Light Source," *Journal of Lightwave Technology*, vol. 9, p. 129 - 134, 1991.

2. J. P. Dakin, C. A. Wade, and P. B. Withers, "An Optical Fiber Pressure Sensor," *SPIE Fiber optics '87:Fifth International Conference on Fiber optics and Opto-electronics*, vol. 734, p. 194 - 201, 1987.

3. J. Farah, "Interferometric Fiber Optic Displacement Sensor," U.S. Patent 5420688, 1995.

4. S. Terry, "A Miniature Silicon Accelerometer with Built-in Damping," *IEEE Solid-State Sensors and Actuators Workshop*, Hilton Head Island, SC, 114, 1988.

5. H. Chau and K. Wise, "An Ultraminiature Solid State Pressure Sensor for a Cardiovascular Catheter," *IEEE Trans. Electron Devices*, vol. 35, p. 2355-2362, 1988.

6. J. A. Folta, N. F. Raley, and E. W. Hee, "Design, Fabrication and Testing of Miniature Peristaltic Membrane Pump," *Tech. Digest IEEE Sensors and Actuators Workshop*, Hilton Head Island, SC, 186, 1992.

7. J. Y. Chang, A. A. Abidi, and M. Gaitan, "Large Suspended Inductors on Silicon and Their Use in a 2 μm CMOS RF Amplifier," *IEEE Electron Device Lett.*, vol. 14, p. 246, 1993.
8. J. H. Jerman, D. J. Clift, and S. R. Mallinson, "A Miniature Fabry-Perot Interferometer With A Corrugated Silicon Diaphragm Support," *Tech. digest IEEE Solid-State Sensor and Actuator Workshop*, p. 140-144, 1990.
9. B. Halg, "A Silicon Pressure Sensor With A Low-cost Contactless Interferometric Optical Readout," *Sensors and Actuators A*, vol. 30, p. 225- 229, 1992.
10. R. A. Wolthuis, G. L. Mitchell, E. Saaski, J. C. Hartl, and M. A. Afromowitz, "Development of Medical Pressure and Temperature Sensors Employing Optical Spectrum Modulation," *IEEE Trans. on Biomedical Engin.*, vol. 38, p. 974 - 980, 1991.
11. K. Aratani, P. J. French, P. M. Sarro, D. Poenar, R. F. Wolffenbuttel, and S. Middelhoek, "Surface Micromachined Tunable Interferometer Array," *Sensors and Actuators*, vol. A 43, p. 17-23, 1994.
12. Y. Kim and D. P. Neikirk, "Micromachined Fabry-Perot cavity based Pressure Transducer," to be published in *IEEE Photonics Technology Letters*, 1995.
13. O. Tabata, K. Kawahata, S. Sugiyama, and I. Igarashi, "Mechanical Property Measurements of Thin Films using Load-Deflection of Composite Rectangular Membranes," *Sensors and Actuators A*, vol. 20, p. 135-141, 1989.
14. Y. Kim and D. P. Neikirk, "Design for Manufacture of Fabry-Perot cavity based Sensors," *Sensors and Actuators A*, August, 1995.
15. M. Born and E. Wolf, *Principles of Optics*. Oxford, England: Pergamon Press, 1980.
16. E. D. Palik, Ed., *Handbook of Optical Constants of Solids*. Orlando, FL: Academic Press, 1985.
17. C. C. Chang and H. D. Conway, "The Marcuse Method Applied to Solution of Uniformly Loaded and Clamped Rectangular Plate Subjected to Forces in Its Plates," *Journal of Applied Mechanics*, vol. 19, p. 179-184, 1952.
18. K. W. Goossen, J. A. Walker, and S. C. Arney, "Silicon Modulator based on Mechanically-active anti-reflection Layer for Fiber-in-the-loop Applications," *Optical Fiber Communications*, San Jose, CA, p.50, 1994.